Aberrant temporal and spatial brain activity during rest in patients with chronic pain

Sanna Malinen[a,b,1], Nuutti Vartiainen[a,b], Yevhen Hlushchuk[a,b], Miika Koskinen[a,b], Pavan Ramkumar[a], Nina Forss[a,c], Eija Kalso[d], and Riitta Hari[a,b,e,1]

[a]Brain Research Unit and [b]Advanced Magnetic Imaging Centre, Low Temperature Laboratory, Aalto University School of Science and Technology, FI-00076 Espoo, Finland; [c]Department of Clinical Neurosciences, [d]Department of Anaesthesia and Intensive Care Medicine, Pain Clinic, and [e]Department of Clinical Neurophysiology, Helsinki University Central Hospital, FI-00029 Helsinki, Finland

Contributed by Riitta Hari, February 5, 2010 (sent for review July 19, 2009)

In the absence of external stimuli, human hemodynamic brain activity displays slow intrinsic variations. To find out whether such fluctuations would be altered by persistent pain, we asked 10 patients with unrelenting chronic pain of different etiologies and 10 sex- and age-matched control subjects to rest with eyes open during 3-T functional MRI. Independent component analysis was used to identify functionally coupled brain networks. Time courses of an independent component comprising the insular cortices of both hemispheres showed stronger spectral power at 0.12 to 0.25 Hz in patients than in control subjects, with the largest difference at 0.16 Hz. A similar but weaker effect was seen in the anterior cingulate cortex, whereas activity of the precuneus and early visual cortex, used as a control site, did not differ between the groups. In the patient group, seed point-based correlation analysis revealed altered spatial connectivity between insulae and anterior cingulate cortex. The results imply both temporally and spatially aberrant activity of the affective pain-processing areas in patients suffering from chronic pain. The accentuated 0.12- to 0.25-Hz fluctuations in the patient group might be related to altered activity of the autonomic nervous system.

functional MRI | insula | resting state | autonomic nervous system | human

Acute pain has an important protective function and is supported by a well-known brain network comprising the insular cortex, anterior cingulate cortex (ACC), primary and secondary somatosensory cortex, and thalamus (1). When pain becomes chronic, its physiological protective function is lost. Chronic pain decreases the quality of life and interferes with the cognitive, affective, and physical functioning. Although one-fifth of the Western population suffers from chronic pain (2), the underlying brain activity is poorly understood.

Extensive meta-analyses (1, 3, 4) indicate that the brain areas related to chronic and acute pain differ to some extent, but no single brain-activity pattern is specific to chronic pain. Morphometric analyses suggest gray-matter loss in many chronic pain conditions, indicating that chronic pain may alter brain structure (5), but in a reversible manner (6).

Previous studies on the brain basis of chronic pain have concentrated on abnormal activation sites and strengths following external stimulation. Studies of resting-state brain activity by means of functional magnetic resonance imaging (fMRI) have shown that the connectivity within the default-mode network (7) is altered in chronic pain, together with reduced task-related deactivation within this network (8, 9). Recently, the spectra of the default-mode network were shown to contain more power at 0.05 to 0.1 Hz in patients suffering from diabetic neuropathic pain than in healthy control subjects (9).

In the present study, we focused on the resting-state fluctuations and functional connectivity of the affective pain-processing areas, the insula and ACC, in chronic pain. Specifically, we recorded spontaneous fMRI signals during rest for about 10 min from 10 patients suffering from different types of spontaneous chronic pain that had lasted, on average, for 10 years (range 1–30 years). The results were compared with an age- and sex-matched control group.

Independent component analysis (ICA) was first applied to fMRI data collected during rest to unravel functionally coupled brain regions, and the analysis was completed with spectral and spatial-correlation analysis of spontaneous fluctuations. As the main finding, the patients had enhanced 0.12- to 0.25-Hz fluctuations and disturbed connectivity in their affective pain matrix.

Results

Pain Ratings. Before scanning, the patients estimated, on a visual analog scale from 0 to 10, the intensity of their continuous pain. The intensity had been 6.4 ± 0.6 (mean ± SEM; range from 2.5–8) during the previous week and was 5.3 ± 0.6 (range 2.5–8) on the day of the measurement. All patients, but none of the control subjects, experienced pain throughout the scanning.

Spatially Independent Components and Their Time Courses. Fig. 1 shows, on an average brain, the patterns of three spatially independent components (ICs) that we studied in detail; the IC analysis was based on the pooled data of patients and control subjects: IC1 (red) showed strongest activity in the lower insular region in both hemispheres, IC2 (green) included the anterior and middle cingulate cortices, IC3 (blue) comprised the precuneus, and early visual cortices (VisCx), and was used as a control.

Fig. 2 shows the corresponding time courses for all patients (*Upper*) and control subjects (*Lower*). The temporal patterns differ already upon visual inspection, both between the three components and between the two subject groups. In the insula and ACC, both groups display rhythmic fluctuations, whereas the signals are more irregular in the precuneus and VisCx. In the insula, the fluctuations are faster in patients than in control subjects, evident from the power spectra displayed in Fig. 3. Although the main spectral power in the control subjects is below 0.12 Hz (corresponding to eight cycles or less per minute), patients have abundant activity at 0.12 to 0.25 Hz, most conspicuous in the insular component. High-resolution analysis of this frequency band indicated that only in the insula and ACC the largest differences between the two groups occured around 0.16 Hz. Control subjects also have some 0.12- to 0.25-Hz activity in the insula.

Fig. 4 shows the total spectral power in both control subjects and patients divided into three frequency bands. In the highest frequency band (0.12–0.25 Hz), the patients have statistically significantly more power than the control subjects in insula and ACC ($P < 0.005$ and $P < 0.006$, respectively), whereas no statistically significant difference is seen in the precuneus and VisCx. In the two lower bands (0–0.05 Hz

Author contributions: S.M., N.V., Y.H., N.F., and R.H. designed research; S.M., N.V., Y.H., M.K., E.K., and R.H. performed research; S.M., N.V., Y.H., M.K., P.R., and R.H. analyzed data; and S.M., N.V., and R.H. wrote the paper.

The authors declare no conflict of interest.

Freely available online through the PNAS open access option.

[1]To whom correspondence should be addressed. E-mail: sanna@neuro.hut.fi; hari@neuro.hut.fi.

This article contains supporting information online at www.pnas.org/cgi/content/full/1001504107/DCSupplemental.

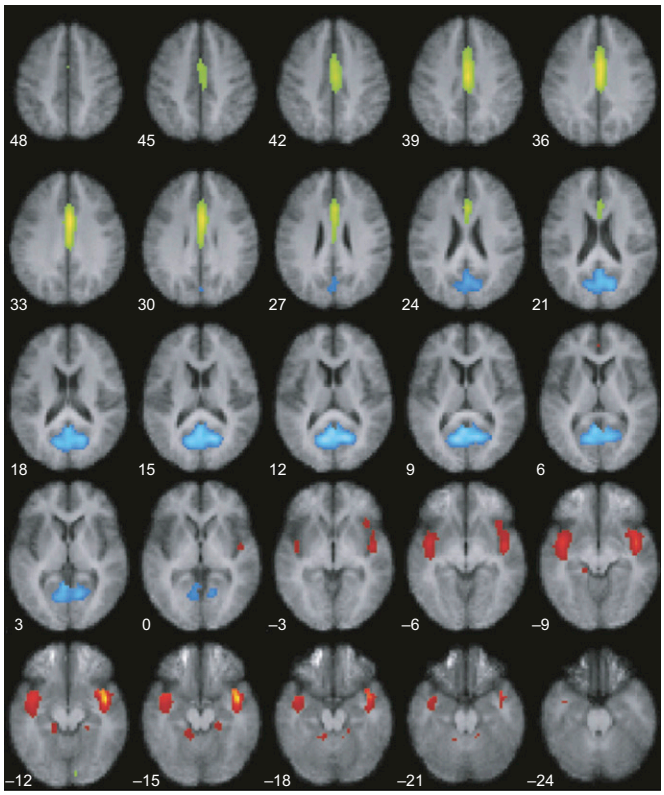

Fig. 1. Spatial patterns of three independent components (MNI *z*-coordinates indicated for the slices). The red color delineates common areas of IC1 in the whole study group (patients plus controls), green/yellow shows IC2, and blue is IC3 used as a control site.

and 0.05–0.12 Hz), the groups behave similarly, except for a small difference in the lower band of the ACC ($P < 0.02$).

Connectivity Analysis. Fig. 5 illustrates the result of correlation analysis based on seed regions in the right and left anterior insula, right middle and left posterior insula, anterior middle cingulate cortex (MCC), posterior ACC, and the VisCx. In control subjects, both the anterior and the posterior insulae were activated bilaterally, and their signals covaried with the ACC regardless of the seed area. In patients, the ACC and insula were not functionally connected.

Table S1 summarizes the statistically significant differences between control subjects and patients. The subject groups differed in all connectivities reported, except when the anterior MCC served as the seed area. The control analysis with the VisCx seed showed no statistically significant differences between the groups within the affective pain matrix. In these analyses, the affective pain matrix never showed greater connectivity in patients than in control subjects.

Discussion

Main Findings. The major abnormalities in our patients suffering from chronic pain were the aberrant temporal fluctuations and disturbed functional connectivity covering the lower insula and ACC, which belong to the affective pain matrix.

In healthy subjects, blood-oxygen-level-dependent (BOLD) fluctuations concentrated within the affective pain matrix, as well as in precuneus and VisCx, to frequencies below 0.1 Hz that have been commonly described to occur during the resting state (10, 11), and the functional connectivity between insula and ACC/MCC was comparable to previous observations (12).

Regular signal fluctuations were observed in the insular regions of both subject groups, although the fluctuations were significantly faster in patients. The regularity, as such, suggests an underlying physiological mechanism that we discuss in greater detail below.

Insular and ACC Activity Related to Pain. The insular cortex is commonly activated in brain-imaging studies of acute experimental pain. During chronic pain, however, the insular activity may be complex. In an early PET study, patients with ongoing neuropathic pain had increased regional cerebral blood flow in bilateral insulae and in the ACC (13), whereas alleviation of postherpetic pain by lidocaine increased activity in the right anterior insula and inferior frontal gyrus, although the other parts of the cerebral pain circuitry were suppressed (14). Similarly, insular (as well as ACC) activity was increased during placebo analgesia (15).

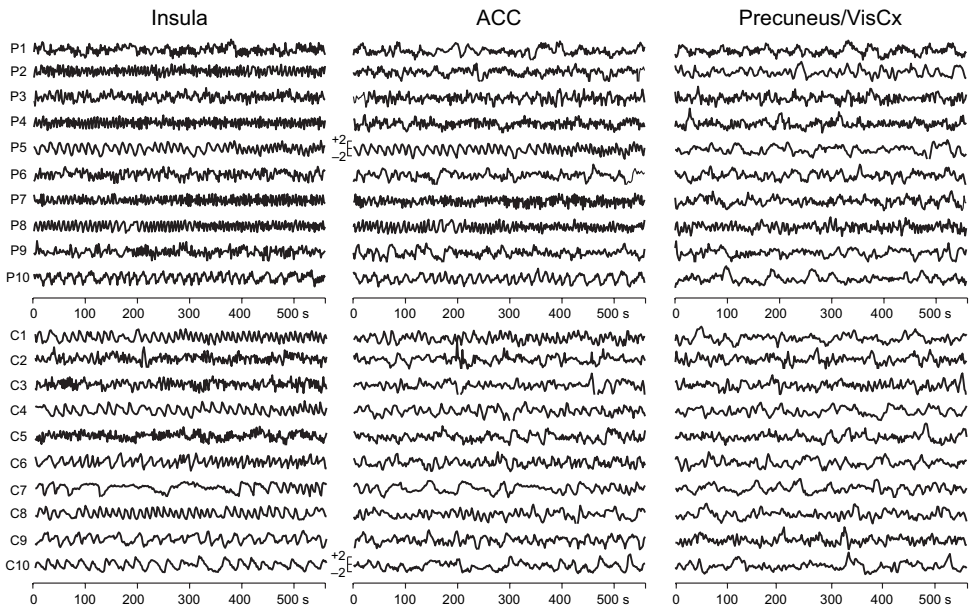

Fig. 2. Individual time courses of ICs 1, 2, and 3 shown separately for all patients (*Upper*, P1–P10) and control subjects (*Lower*, C1–C10).

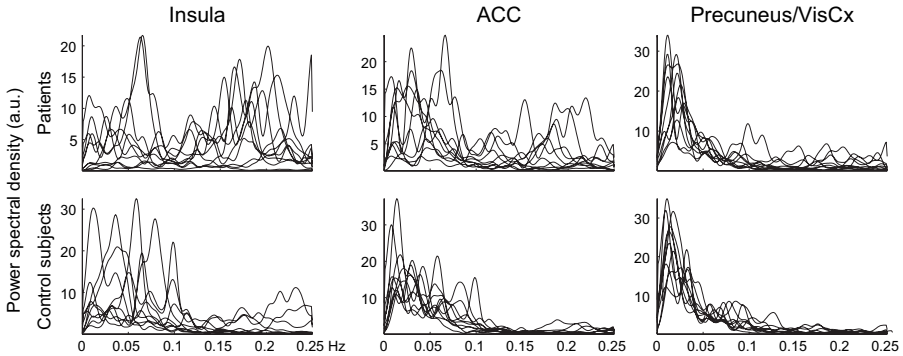

Fig. 3. Individual normalized spectra superimposed separately for patients (*Upper*) and control subjects (*Lower*).

Current consensus emphasizes the role of insula for interoception (16, 17). Electrical stimulation of human insular cortex elicits, in addition to pain, auditory, vestibular, vegetative, olfactory, and gustatory responses, thereby implying a multimodal role for the insular cortex (18). Insula receives afferent connections from a multitude of cortical areas, including primary and secondary somatosensory cortex, orbitofrontal cortex, cingulate gyrus, and associative cortices (19). It also receives input from the autonomic nervous system (ANS), and its role in autonomic function is supported by connections to amygdala, hypothalamus, and cingulate cortex. Insular lesions (after a stroke, for example) may lead to cardiac complications, assumed to take place via changed ANS function (20). Because interoception, homeostasis, and pain are closely connected (21), our pain patients' accentuated oscillations in insular cortices and ACC could reflect modulations in ANS function associated with continuous activity of the nociceptive system.

Nociceptive pathways project to midbrain and brain-stem areas that regulate ANS function (22). Pain, and even anticipation of pain, can elicit ANS arousal. Long-term noxious bombardment may result in ANS dysfunction, and such disorders have been found in patients suffering from various clinical pain conditions, such as chronic tension headaches and migraines (23), as well as irritable bowel syndrome and chronic pelvic pain syndrome (24, 25). It is thus tempting to speculate that the accentuation of insular and ACC oscillations in our patients were related to modified autonomic arousal driving the cerebral hemodynamics.

It is also to be noted that, whereas insula and ACC were functionally connected in our healthy subjects, the connectivity was restricted in the patient group. In healthy subjects, the anterior insula–ACC system has been suggested to integrate the interoceptive input with its emotional salience in contrast to the whole insula–MCC system, which is more related to environmental monitoring and response selection (12). In our patients, the observed disruption of the connectivities of both these systems could result from constant noxious input, although this result contradicts recent findings in patients with diabetic neuropathic pain, whose functional connectivity was strengthened in networks including, for example, anterior insula (9).

Possible Sources of Artifacts. Physiological signals arising, for example, from cardiac function, respiration, or blood pressure, can have substantial impact on the measured BOLD signal. The sites of origin of these fluctuations can overlap with functional networks fluctuating during rest and methods such as principal component analysis or ICA may not be able to separate the neural activity from the physiological noise sources (26).

Cardiac cycle-related artifacts in BOLD fMRI can be observed in several brain regions (27). To avoid such physiological noise, many recent studies of the resting-state networks have focused on frequencies below 0.1, or even below 0.08 Hz (28–30). Cardiac-gated data acquisition (31, 32), or modeling and correcting for respiration and heart-cycle artifacts, can improve the statistical power of the data analysis (33–36).

The main cardiac cycle-related artifacts occur close to large vessels (27) at 0.6 to 1.3 Hz in the typical BOLD spectrum (11). In our study, the strongest fluctuations occurred close to the course of medial cerebral artery, but importantly also included other areas, such as the ACC. To understand the possible effect of cardiac function on the insular BOLD signal fluctuations, we carried out control fMRI–ECG recordings on two healthy subjects and on two patients (*SI Text*). Despite a weak (~0.1) positive correlation between heart rate and BOLD signal, we were not able to distinguish the patients from the control subjects with this measure.

The analgesic medication could have influenced the BOLD fluctuations. Eight of our 10 patients used either gabapentin or pregabalin, which act on voltage-sensitive calcium channels (37). In anesthetized rats, gabapentin modulates the BOLD signal in several areas involved in nociceptive processing, for example, by increasing activity in thalamus and periaqueductal gray matter and decreasing it in amygdala (38). In humans, even a single dose of gabapentin can modulate brain responses to noxious mechanical stimuli (39). Moreover, half of our patients used tricyclic antidepressants

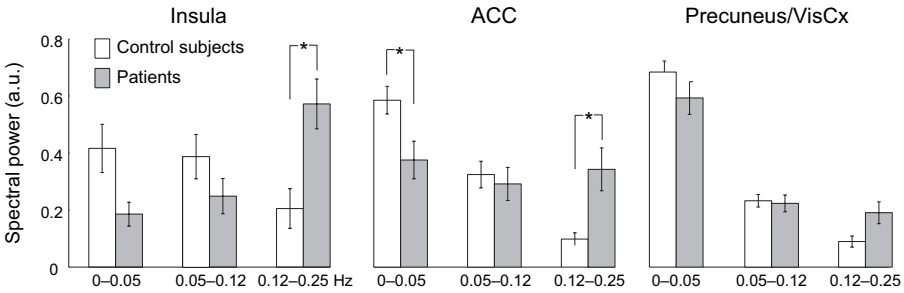

Fig. 4. Mean ± SEM spectral power for the independent components for patients (white bars) and control subjects (gray bars).

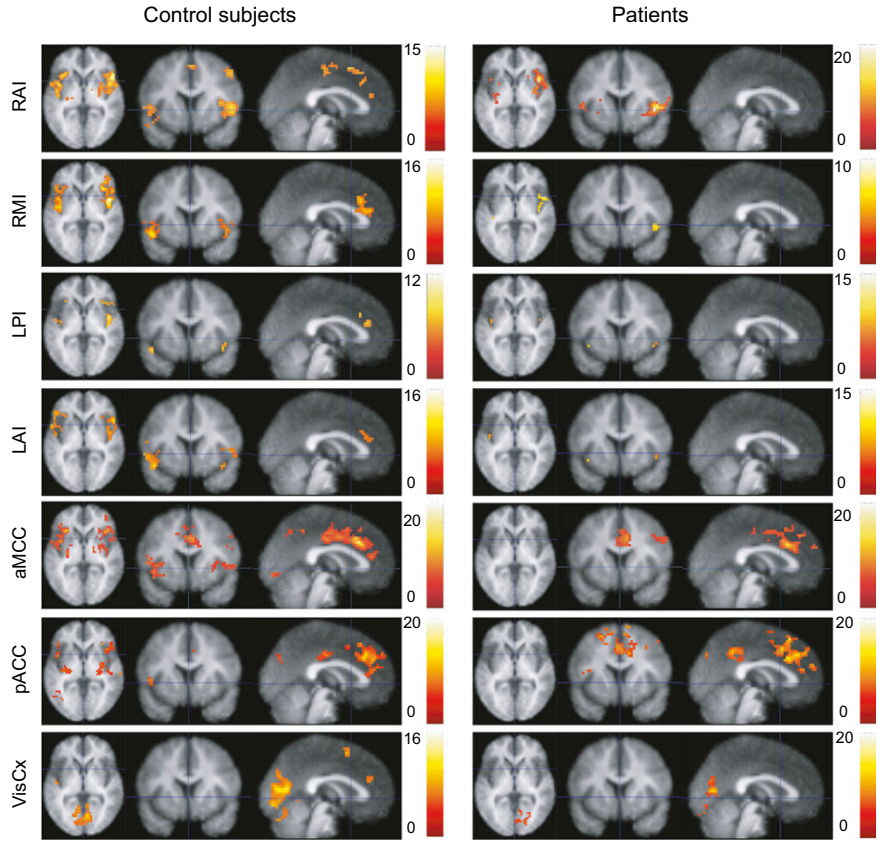

Fig. 5. Spatial connectivity maps (*t* test, $P < 0.0001$ and extent of 20 voxels), seed-point is either right anterior insula (RAI), right middle insula (RMI), left posterior insula (LPI), left anterior insula (LAI), anterior middle cingulate cortex (aMCC), posterior anterior cingulate cortex (pACC), or visual cortex (VisCx).

(amitriptylin or nortriptylin), often administered in low doses to treat chronic pain. These drugs inhibit the reuptake of noradrenaline and serotonine, but can also affect the ANS mainly via anticholinergic effects. The possible effects of all these drugs on the observed BOLD fluctuations still remain to be shown.

Functional Relevance of the 0.1- to 0.25-Hz Fluctuations. The sites of enhanced high-frequency fluctuations are in good agreement with recent findings on functional connectivity in resting healthy subjects (40): a strong coherence in the high-frequency (0.17–0.25 Hz) and the middle-frequency band (0.08–0.17 Hz) was observed in insula and amygdala, whereas the connectivity at the low (below 0.08 Hz) frequencies had different spatial distribution.

Modulation of temporal fluctuations has been observed within the resting-state networks of schizophrenic subjects (41), with accentuation of frequencies from 0.08 to 0.24 Hz, and with the main difference between patients and a healthy control group around 0.13 Hz. This alteration was interpreted to reflect a change in the functional connectivity of the involved brain regions. Similarly, we could explain our results by decreased functional connectivity of the affective-emotional pain matrix in our patient group; this interpretation is supported by the seed-based connectivity analyses.

One possible explanation for the difference between the groups could be modified vasomotion (cyclic variation of the diameter of arterioles) in the activated brain regions, typically occurring around 0.1 Hz (10, 42). However, the exact relationship between local vasomotion and, for example, the ANS drive as a possible synchronization mechanism of arteriolar diameter variations still remains an open question.

Conclusions. The regularly occurring BOLD oscillations in our subjects lead us to propose that the accentuated fluctuations at 0.12 to 0.25 Hz in patients suffering from chronic pain could reflect modulated autonomic arousal. These findings emphasize the importance of closer scrutiny of the time courses of brain activity, an aspect that has been so far quite rare in the fMRI community.

The results also open several questions for future research. For example, we need information about the influence of various drugs on the BOLD fluctuations. Moreover, it would be beneficial to routinely monitor variability in ANS function during the fMRI scanning to illuminate the extent to which intrinsic BOLD fluctuations really reflect ANS activity.

Materials and Methods

Subjects. We studied 10 patients (ages 38–67 years, mean 51; eight males, two females) who suffered from a continuous spontaneous chronic pain. Table S2 lists the site, etiology, duration, and intensity of the pain in each patient; Table S3 lists the medications.

All patients suffered from spontaneous severe pain. They were recruited from the Pain Clinic of the Helsinki University Central Hospital. Ten healthy subjects matched for age and sex (37–64 years, mean 50; eight males, two females) served as control subjects who reported no neurological disorders or chronic pain conditions.

fMRI Setup and Image Acquisition. The images were acquired with a 3-T magnet (SIGNA EXCITE 3.0 T scanner; GE Healthcare) at the Advanced Magnetic Imaging Centre of Aalto University School of Science and Technology. Each subject signed an informed consent before entering the scanner. The recordings had a prior approval by the Ethics Committee of the Helsinki and Uusimaa Hospital District.

The subjects had no other task but to stay alert and to keep the eyes open during the 10-min scanning run.

The images were acquired using a gradient-echo echo planar-imaging sequence with the following parameters: time to repeat (TR) 2,000 ms, echo time (TE) 32 ms, flip angle (FA) 75°, field-of-view 20 cm, and matrix size 64 × 64. In total, 33 oblique slices were acquired in an interleaved fashion to cover

the whole brain. The slices were 4-mm thick, with no spacing in-between. One 10-min run included 284 brain volumes, of which the first 4 were discarded to allow for stabilization of the T1-relaxation effects.

For combining the functional data with anatomical data, high-resolution anatomical images were obtained with 3D fast spoiled-gradient echo sequence (inversion-recovery prepared): TR 9 ms, TE 1.9 ms, FA 15°, 256 × 256 matrix, field-of-view 26 cm, slice thickness 1 mm.

Preprocessing. The fMRI data were preprocessed with statistical parametric mapping software SPM2 (http://www.fil.ion.ucl.ac.uk/spm/), including realignment, normalization into the Montreal Neurological Institute (MNI) standard space (skull was stripped prior the normalization), and smoothing with a 6-mm (full-width at half-maximum) Gaussian filter. The maximum translational head motion was in both groups smaller than the voxel size, namely 1.6 mm in the control subjects and 1.0 mm in the patients. In addition, the rotations were small: 0.03 degrees at maximum in both groups. We observed no statistically significant differences in the average magnitude of head motion between the groups.

Independent Component Analysis. The ICs were identified using GIFT software (http://icatb.sourceforge.net) and group-ICA approach (43). Data from all subjects were concatenated together and 48 common ICs were calculated using the FastICA-algorithm (44, 45) included in the software package.

Two pain-processing network-related ICs, IC1 including the insula bilaterally, and IC2 including the ACC–MCC, were selected for further analysis; IC3, covering both the precuneus and VisCx, was used as a control site.

Power Spectra. Power-density frequency spectra were calculated using the Welch's method, and each individual spectrum was normalized by dividing it by the total signal power. For quantification, the spectra were divided into three frequency bands: 0 to 0.05, 0.05 to 0.12, and 0.12 to 0.25 Hz, and comparisons between the patient and control groups were made with two-sample *t* test.

Analysis of Functional Connectivity. Inter-area correlations were analyzed with respect to predefined regions of interest. A total of seven seed points (spheres of 6-mm radius) were determined from the normalized group data from (*i*) right anterior insula (MNI coordinates 51 15 3) and (*ii*) left anterior insula (–45 6 9), respectively, (*iii*) right middle insula (45 0 6) and (*iv*) left posterior insula (–42 –12 –9), (*v*) aMCC (6 21 33), (*vi*) pACC (3, 33, 36), and (*vii*) the early VisCx (–6 –72 12), clearly outside the known pain-processing circuitry. From these seed points, the raw (preprocessed) data were extracted for each individual separately using MarsBaR-software (http://marsbar.sourceforge.net). Each extracted average time course was then used as a regressor in a general linear model analysis to reveal the individual connectivity maps.

Individual connectivity maps were subjected to one-sample *t* test (patients and controls separately, threshold uncorrected $P < 0.0001$ and extent of 20 voxels) and differences between the groups were tested with two-sample *t* test ($P < 0.001$ and extent of 20 voxels).

ACKNOWLEDGMENTS. This work was supported by the Academy of Finland (National Centers of Excellence Program 2006–2011), the Sigrid Jusélius Foundation, the Jenny and Antti Wihuri Foundation, European Research Council Advanced Grant 232946, the Ministry of Education via the Finnish Graduate School of Neuroscience, and special government grants for health sciences research for the Pain Clinic, Department of Anesthesiology and Intensive Care Medicine, and for the Department of Clinical Neurophysiology, Helsinki University Central Hospital.

1. Apkarian AV, Bushnell MC, Treede RD, Zubieta JK (2005) Human brain mechanisms of pain perception and regulation in health and disease. *Eur J Pain* 9:463–484.
2. Breivik H, Collett B, Ventafridda V, Cohen R, Gallacher D (2006) Survey of chronic pain in Europe: prevalence, impact on daily life, and treatment. *Eur J Pain* 10:287–333.
3. Derbyshire SW (1999) Meta-analysis of thirty-four independent samples studied using PET reveals a significantly attenuated central response to noxious stimulation in clinical pain patients. *Curr Rev Pain* 3:265–280.
4. Peyron R, Laurent B, García-Larrea L (2000) Functional imaging of brain responses to pain. A review and meta-analysis (2000). *Neurophysiol Clin* 30:263–288.
5. May A (2008) Chronic pain may change the structure of the brain. *Pain* 137:7–15.
6. Rodriguez-Raecke R, Niemeier A, Ihle K, Ruether W, May A (2009) Brain gray matter decrease in chronic pain is the consequence and not the cause of pain. *J Neurosci* 29: 13746–13750.
7. Fox MD, Raichle ME (2007) Spontaneous fluctuations in brain activity observed with functional magnetic resonance imaging. *Nat Rev Neurosci* 8:700–711.
8. Baliki MN, Geha PY, Apkarian AV, Chialvo DR (2008) Beyond feeling: chronic pain hurts the brain, disrupting the default-mode network dynamics. *J Neurosci* 28:1398–1403.
9. Cauda F, et al. (2009) Altered resting state in diabetic neuropathic pain. *PLoS One* 4:e4542.
10. Auer DP (2008) Spontaneous low-frequency blood oxygenation level-dependent fluctuations and functional connectivity analysis of the 'resting' brain. *Magn Reson Imaging* 26:1055–1064.
11. Cordes D, et al. (2001) Frequencies contributing to functional connectivity in the cerebral cortex in "resting-state" data. *AJNR Am J Neuroradiol* 22:1326–1333.
12. Taylor KS, Seminowicz DA, Davis KD (2009) Two systems of resting state connectivity between the insula and cingulate cortex. *Hum Brain Mapp* 30:2731–2745.
13. Hsieh JC, Belfrage M, Stone-Elander S, Hansson P, Ingvar M (1995) Central representation of chronic ongoing neuropathic pain studied by positron emission tomography. *Pain* 63:225–236.
14. Geha PY, et al. (2007) Brain activity for spontaneous pain of postherpetic neuralgia and its modulation by lidocaine patch therapy. *Pain* 128:88–100.
15. Petrovic P, Kalso E, Petersson KM, Ingvar M (2002) Placebo and opioid analgesia—imaging a shared neuronal network. *Science* 295:1737–1740.
16. Critchley HD (2004) The human cortex responds to an interoceptive challenge. *Proc Natl Acad Sci USA* 101:6333–6334.
17. Craig AD (2009) How do you feel—now? The anterior insula and human awareness. *Nat Rev Neurosci* 10:59–70.
18. Mazzola L, Isnard J, Mauguière F (2006) Somatosensory and pain responses to stimulation of the second somatosensory area (SII) in humans. A comparison with SI and insular responses. *Cereb Cortex* 16:960–968.
19. Augustine JR (1996) Circuitry and functional aspects of the insular lobe in primates including humans. *Brain Res Brain Res Rev* 22:229–244.
20. Oppenheimer S (2007) Cortical control of the heart. *Cleve Clin J Med* 74 (Suppl 1):S27–S29.
21. Tracey I, Mantyh PW (2007) The cerebral signature for pain perception and its modulation. *Neuron* 55:377–391.
22. Willis WD, Westlund KN (1997) Neuroanatomy of the pain system and of the pathways that modulate pain. *J Clin Neurophysiol* 14:2–31.
23. Sliwka U, et al. (2001) Spontaneous oscillations in cerebral blood flow velocity give evidence of different autonomic dysfunctions in various types of headache. *Headache* 41:157–163.
24. Tousignant-Laflamme Y, Goffaux P, Bourgault P, Marchand S (2006) Different autonomic responses to experimental pain in IBS patients and healthy controls. *J Clin Gastroenterol* 40:814–820.
25. Yilmaz U, Liu YW, Berger RE, Yang CC (2007) Autonomic nervous system changes in men with chronic pelvic pain syndrome. *J Urol* 177:2170–2174.
26. Birn RM, Murphy K, Bandettini PA (2008) The effect of respiration variations on independent component analysis results of resting state functional connectivity. *Hum Brain Mapp* 29:740–750.
27. Dagli MS, Ingeholm JE, Haxby JV (1999) Localization of cardiac-induced signal change in fMRI. *Neuroimage* 9:407–415.
28. Fox MD, et al. (2005) The human brain is intrinsically organized into dynamic, anticorrelated functional networks. *Proc Natl Acad Sci USA* 102:9673–9678.
29. Fransson P (2006) How default is the default mode of brain function? Further evidence from intrinsic BOLD signal fluctuations. *Neuropsychologia* 44:2836–2845.
30. Greicius MD, Srivastava G, Reiss AL, Menon V (2004) Default-mode network activity distinguishes Alzheimer's disease from healthy aging: evidence from functional MRI. *Proc Natl Acad Sci USA* 101:4637–4642.
31. Guimaraes AR, et al. (1998) Imaging subcortical auditory activity in humans. *Hum Brain Mapp* 6:33–41.
32. Malinen S, Schürmann M, Hlushchuk Y, Forss N, Hari R (2006) Improved differentiation of tactile activations in human secondary somatosensory cortex and thalamus using cardiac-triggered fMRI. *Exp Brain Res* 174:297–303.
33. Birn RM, Smith MA, Jones TB, Bandettini PA (2008) The respiration response function: the temporal dynamics of fMRI signal fluctuations related to changes in respiration. *Neuroimage* 40:644–654.
34. Chang C, Cunningham JP, Glover GH (2009) Influence of heart rate on the BOLD signal: the cardiac response function. *Neuroimage* 44:857–869.
35. Glover GH, Li TQ, Ress D (2000) Image-based method for retrospective correction of physiological motion effects in fMRI: RETROICOR. *Magn Reson Med* 44:162–167.
36. Shmueli K, et al. (2007) Low-frequency fluctuations in the cardiac rate as a source of variance in the resting-state fMRI BOLD signal. *Neuroimage* 38:306–320.
37. Dooley DJ, Taylor CP, Donevan S, Feltner D (2007) Ca2+ channel alpha2delta ligands: novel modulators of neurotransmission. *Trends Pharmacol Sci* 28:75–82.
38. Governo RJ, Morris PG, Marsden CA, Chapman V (2008) Gabapentin evoked changes in functional activity in nociceptive regions in the brain of the anaesthetized rat: an fMRI study. *Br J Pharmacol* 153:1558–1567.
39. Iannetti GD, et al. (2005) Pharmacological modulation of pain-related brain activity during normal and central sensitization states in humans. *Proc Natl Acad Sci USA* 102:18195–18200.
40. Salvador R, et al. (2008) A simple view of the brain through a frequency-specific functional connectivity measure. *Neuroimage* 39:279–289.
41. Garrity AG, et al. (2007) Aberrant "default mode" functional connectivity in schizophrenia. *Am J Psychiatry* 164:450–457.
42. Mayhew JE, et al. (1996) Cerebral vasomotion: a 0.1-Hz oscillation in reflected light imaging of neural activity. *Neuroimage* 4:183–193.
43. Calhoun VD, et al. (2001) A method for making group inferences from functional MRI data using independent component analysis. *Hum Brain Mapp* 14:140–151.
44. Hyvärinen A (1999) Fast and robust fixed-point algorithms for independent component analysis. *IEEE Trans Neural Netw* 10:626–634.
45. Hyvärinen A, Oja E (1997) A fast fixed-point algorithm for independent component analysis. *Neural Comput* 9:1483–1492.

Supporting Information

Malinen et al. 10.1073/pnas.1001504107

SI Text

Additional fMRI–ECG Measurements. Two patients and two control subjects participated in an additional functional MRI (fMRI) measurement, in which the subject's heart rate was simultaneously recorded.

Two channels of ECG (sampling frequency, 250 Hz) were measured with magnet-compatible electrodes along with photoplethysmography and respiration signals with an integrated amplifier in the fMRI scanner. The ECG was adjusted with the fMRI signal off-line; data were low-pass filtered (12 Hz) and R-peaks were enhanced by multiplying the ECG signal with the time-shifted photoplethysmography signal. Optionally, time-domain independent component analysis was used to improve the R-peak detection. The resulting RR time-series was finally visually approved.

The mean fMRI signal of the specific regions of interest (ROIs) (*Analysis of functional connectivity* in *Materials and Methods*) and the corresponding RR time-series were interpolated into 2-Hz sampling frequency. The mutual dependencies of the signals were studied by computing their cross-correlations.

Correspondingly, respiration signal, adjusted with the fMRI in time-domain, was downsampled to 2 Hz and cross-correlated with ROI signals.

The heart rates varied from 54 to 65 beats per min, and no systematic dependence between signal variability and heart or respiration rate could be determined. Furthermore, time-lagged correlations between ROI signals and RR time-series showed similar correlation profiles across different ROIs of each individual.

Table S1. Statistically significant differences between patients and controls

Seed	L Insula	R Insula	ACC
RAI	+	−	−
RMI	−	+	−
LPI	−	−	+
LAI	−	−	+
aMCC	−	−	−
pACC	+	+	+
VisCx	−	−	−

Statistically significant differences ($P < 0.001$) between patients and control control subjects in connectivities between different seed regions and left (L) insula, right (R) insula, and ACC. Anterior cingulate cortex, ACC; anterior middle cingulate cortex, aMCC; left anterior insula, LAI; left posterior insula, LPI; right anterior insula, RAI; posterior anterior cingulate cortex, pACC; right middle insula, RMI; visual cortex, VisCx.

Table S2. Clinical details of the patients

						Intensity	
Patient no.	Age (yr)	Sex	Site of pain	Etiology	Duration (yr)	Week	Day
1	54	M	R upper limb	Cervical spine degeneration	16	7	5
2	46	M	R lower limb	CRPS II	16	5.5	5.5
3	46	M	R lower limb	Posttraumatic osteoarthritis	2	7	3
4	48	M	R upper limb	Unclear	3	7	5
5	54	F	Lumbar spine	Lumbar spine degeneration	18	2.5	2.5
6	38	M	Lumbar spine	Lumbar spine degeneration	1	8	6.5
7	63	M	L upper limb	Phantom limb pain	30	8	8
8	41	F	Lumbar spine	Lumbar spine degeneration	4	5	5
9	50	M	Lumbar spine	Lumbar spine degeneration	2	8	8
10	67	M	Both knees	Postsurgical	3	5.5	4

F, female; L, left; M, male; R, right. Mean intensity of pain during the last week and on the day of the measurement is given on a 0 to 10 scale, where 0 is no pain at all and 10 is the worst pain imaginable.

Table S3. Medication of all 10 patients

Patient no.	Daily doses of drugs used for pain relief	Other drugs
1	Acetaminophen 500 mg + codeine 30 mg × 4	Candesartan 16 mg × 1 for hypertension
2	Pregabalin 25 mg × 2, amitriptyline 20 mg × 1	
3	Gabapentin 800 mg × 4, amitriptyline 100 mg × 1, tramadol 150 mg × 1	
4	Amitriptyline 12.5 + 75 mg	Nifedipine 20 mg × 1 for hypertension
5	Pregabalin 100 mg × 1	
6	Pregabalin 150 mg x 2, nortriptyline 50 mg × 1	
7	Pregabalin 150 mg x 2, acetaminophen 500 mg + codeine 30 mg 2 × 3–4	
8	Ibuprofen 800 mg x 2, acetaminophen 500 mg + codeine 30 mg 1–2 × 1–4, pregabalin 25 + 75–100 mg	Bisoprolol 2.5 mg × 1 for cardiac insufficiency
9	Mirtazapine 15 mg x 1, buprenorphine 0.4 mg × 2–3, pregabalin 150 mg × 2, nortriptyline 50 mg × 1	Ramipril 2.5 mg x 1 + hydrochlortiazide 12.5 mg x 1 + amlodipine 5 mg × 1 for hypertension
10	Gabapentin 300 mg × 2, tramadol 150 mg × 1, acetaminophen 500 mg + codeine 30 mg × 1	